HHS Public Access

Author manuscript

Radiat Res. Author manuscript; available in PMC 2020 March 17.

Published in final edited form as:

Radiat Res. 2018 January ; 189(1): 53–63. doi:10.1667/RR14843.1.

Effects of $^{1}H+^{16}O$ Charged Particle Irradiation on Short Term Memory and Hippocampal Physiology in a Murine Model

Frederico Kiffer[1,2,a], **Hannah Carr**[1,2], **Thomas Groves**[1,2,3], **Julie E. Anderson**[1,2], **Tyler Alexander**[1,2,a], **Jing Wang**[1,2], **John W. Seawright**[1,2], **Vijayalakshmi Sridharan**[1,2], **Gwendolyn Carter**[1,2], **Marjan Boerma**[1,2], **Antiño R. Allen**[1,2,3,#]

[1]Division of Radiation Health, University of Arkansas for Medical, Sciences, Little Rock, AR 72205

[2]Department of Pharmaceutical Sciences, University of Arkansas for Medical, Sciences, Little Rock, AR 72205

[3]Center for Translational Neurobiology & Developmental Sciences, University of Arkansas for Medical, Sciences, Little Rock, AR 72205

Abstract

Radiation from galactic cosmic rays (GCR) poses a significant health risk for deep-space flight crews. GCR are unique in their extremely high-energy particles. Because of current spacecraft shielding technology, some of the predominant particles astronauts would be exposed to are ^{1}H + ^{16}O. Radiation has been shown to cause cognition deficits in mice. The hippocampus plays a key role in memory and cognitive tasks in that it receives information from the cortex, undergoes dendritic-dependent processing, and then relays information back to the cortex. The aim of our study is to investigate the effects of combined ^{1}H + ^{16}O irradiation on cognition and dendritic structures in the hippocampus of adult male mice three months postirradiation. Six-month old male C57BL/6 mice were irradiated first with ^{1}H (.5Gy, 150MeV/n) and one hour after with ^{16}O (.1Gy, 600MeV/n) at the NASA Space Radiation Laboratory in Upton, NY. Three months after irradiation, animals were tested for hippocampus-dependent cognitive performance in the Y-maze test. Upon sacrifice, molecular and morphological assessments were conducted on hippocampal tissues. During Y-maze testing, mice exposed to radiation failed to distinguish the novel arm, spending approximately the same amount of time in all three arms during the retention trial relative to sham. Irradiated animals also showed changes in expression of glutamate receptor subunits and synaptic density-associated proteins. ^{1}H + ^{16}O irradiation compromised dendritic morphology in the cornu ammonis 1 and dentate gyrus within the hippocampus. These data indicate cognitive injuries due to ^{1}H + ^{16}O 3 months post-irradiation.

[#]Corresponding author: Dr. Antiño R. Allen, University of Arkansas for Medical Sciences, 4301 West Markham, Suite 441B-2, Little Rock, AR 72205, Phone: 501-686-7553, Fax: 501-526-6599, Aallen@uams.edu.

[a]Scholar in Training.

Author Contributions:

Conceived and designed the experiments: ARA, FK. Performed the Experiments: ARA, FK, HC, TG, JEA, TA, JWS, VS. Analyzed the data: ARA, FK, JW, GC. Contributed reagents/materials/analysis tools: ARA, MB. Wrote the paper: ARA, FK.

Competing Interest: None of the authors has competing financial interests or other conflicts of interst

Keywords

radiation; hippocampus; dendritic spines

INTRODUCTION

The future of manned space exploration relies on understanding the health risks of long-term deep-space missions. A variety of conditions pose hazards to human health in the deep-space environment, chief among them is the radiation environment. The primary sources of radiation includes galactic cosmic rays (GCR) and solar particle events (SPE). GCR consist of the high-energy charged nuclei of approximately 87% hydrogen, 12% helium, and 1-2% high-mass (Z > 2), high-energy (HZE) particles.(1) SPE are composed of mostly energetic protons (^{1}H).(2) Although minimal in relative abundance, HZE particles contribute to as much as 20% of the total Mars-relevant total organ radiation dosage in deep space, while from GCR alone deliver approximately 50-60% of radiation.(3–6) Electromagnetic radiation, such as gamma and x-rays, is effectively absorbed by spacecraft; however, there is currently no feasible shield capable of mitigating the charged-particle radiation dosage encountered en route to Mars and beyond.(7)

Data from the Curiosity rover during its transfer orbit aboard the Mars Science Laboratory and after its landing in the Martian Gale crater for approximately 300 days, near the solar maximum of cycle 24, has revealed an average radiation dosage of 0.21 ± .04 mGy/day on the surface and 0.48 ± .08 mGy/day during transfer orbit. These data suggest that a dose equivalent estimate of radiation for a mission with 360 days of cruise and 500 days on the surface of Mars is approximately 1.06 Sv.(4, 5) In order to further understand the threats to human health during space exploration, NASA has instituted a Human Research Roadmap, which embraces the possibility that central nervous system (CNS) damage may occur, and the risk of acute and late CNS effects from space radiation has been outlined as a key area of research. NASA has recently defined permissible CNS exposure limits of 500 mGy for 30 days, 1,000 mGy for 1 year, and 1,500 mGy for a career. NASA also limits CNS exposure to charged particles (Z > 10) to 1-year and career dose exposure limits are 100 mGy and 250 mGy.(d) Due to the high-risk tasks demanded of astronauts on a mission to Mars, the intactness of their cognitive faculties may prove critical to mission success.

Recent studies have shown that exposure to HZE particles impaired animal cognitive behavior. Mice exposed to ^{16}0 (.3Gy) and ^{48}Ti (.05, .3Gy) failed to discriminate between novel and familiar objects during the novel object recognition (NOR) test and had reduced preference to explore novelty during the object in place tasks.(8) Rats irradiated with ^{56}Fe spent less time in the platform quadrant than sham, and they failed to distinguish a novel object in the Morris Water Maze (MWM) and NOR tests, respectively.(9, 10) Exposure to ^{1}H has yielded similar results. Irradiated mice showed cognitive impairment during the MWM.(11) However, there is a paucity of research exploring the combination of and HZE particles on the CNS. To date, only one study assesses whether HZE particles in combination with ^{1}H affected cognitive behavior. Researchers found that mice irradiated with ^{1}H alone (.1 Gy) and with ^{1}H followed one day later by ^{56}Fe (.5 Gy) failed to

distinguish between a novel and familiar object in NOR, whereas the cohort irradiated solely by ^{56}Fe (.5Gy) showed no deficits. These findings suggest that ^{1}H were responsible for the impairment.(12) The aim of the present study is to investigate how whole body mixed field ^{1}H + ^{16}O irradiation within one day affects hippocampus-dependent cognitive performance and dendritic complexity 3 months postexposure.

MATERIALS AND METHODS

Animals and Irradiation

All animal procedures were approved by the Institutional Animal Care and Use Committees of the University of Arkansas for Medical Sciences (UAMS) and Brookhaven National Laboratory (BNL). Sample sizes in this study were n=10 per treatment group, and every assay involved samples from mice that underwent behavioral testing. Male C57BL/6 mice were obtained from Jackson Laboratory (Bar Harbor, ME) and were housed 5 per cage. Throughout the duration of the study, mice received standard rodent chow that was low in soy (2020X, Harlan Laboratories), water *ad libitum*, and were housed on a 12:12 hour light:dark cycle. At 6 months of age, mice were transported to BNL by overnight airlift. At BNL, mice were again administered the 2020X diet, water *ad libitum*, and were housed on a 12:12 hour light:dark cycle. After a one week acclimation, mice were exposed to whole-body irradiation at the NASA Space Radiation Laboratory (NSRL) at BNL. For this purpose, mice were individually placed in well-ventilated clear Lucite cubes, and then placed within the NSRL beam line, 5 mice at the time. Mice received a single dose of ^{1}H (150 MeV, 0.5 Gy, 18-19 cGy/min), and immediately after exposure, mice were placed back in their cage. An hour later, all mice were placed in Lucite cubes a second time and exposed to whole-body ^{16}O (600 MeV/n, 0.1 Gy, 18-33 cGy/min). Radiation dosimetry was performed by the NSRL physics team. Sham-irradiated mice were also transported to NSRL and placed in clear Lucite cubes, but were not exposed to ^{1}H or ^{16}O. Two days after irradiation or sham treatment, mice were returned to UAMS by overnight airlift. Upon return, mice were administered 2020X chow, containing 150 ppm fenbendazole, for 8 weeks, as a routine UAMS quarantine procedure.

Y-maze

The Y-maze assessed short-term spatial memory and exploratory activity in a novel environment.(13) It consisted of three acrylic glass arms (45 × 15 × 30 cm), each designated as either the starting arm, the novel arm, or the familiar arm. The test consisted of two different trials that were performed 4 hours apart. Before the experiment, animals (n=10) were assigned to two arms (start and familiar) to which they were exposed during the first phase of the test (training trial). A unique object was secured at the end of each arm to differentiate start, familiar, and novel arms. Allocation of arms (start, familiar, and novel) was counterbalanced within each experimental group. During the training trial, mice were put at the end of the start arm and allowed to freely move and explore the start and familiar arm for 5 minutes. The novel arm was blocked during the training trial. After 4 hours, the second trial (testing trial) was performed during which mice had free access to all three arms and were allowed to explore the Y-maze for 5 minutes. Each session was recorded on a

charge-coupled device video camera, located above the maze for automatic behavioral analysis with EthoVision software version 11 (Noldus Information Technology).

RNA Extraction and Quantitative Reverse Transcription Polymerase Chain Reaction (qRT-PCR)

After behavioral tests, mice were anesthetized by isoflurane inhalation, and hippocampi were dissected from each treatment group (n=10 per group), immediately frozen in liquid nitrogen, and subsequently stored at −80°C. Total RNA was extracted from hippocampal tissue with the AllPrep DNA/RNA extraction kit (QIAGEN, Valencia, CA), according to the manufacturer's protocol. RNA quality and quantity was assessed on a Nanodrop 2000 instrument (Thermo Scientific, Waltham, MA). cDNA was synthesized with random primers and a high-capacity cDNA reverse transcription kit (Applied Biosystems, Foster City, CA), according to the manufacturer's protocol (Life Technologies, Grand Island, NY). The levels of gene transcripts were determined by qRT-PCR with TaqMan Gene Expression Assays (Life Technologies, and Integrated DNA Technologies, Coralville, IA), according to the manufacturer's protocol. In all cases, *GAPDH* was used as an internal reference gene, and fold changes were calculated with the 2-ddCt method. Measurements were taken in triplicates.

Golgi Staining

To establish the impact of $^{16}0 + {}^{1}H$ on mature neuronal morphology, brains from mice exposed to $^{16}O + {}^{1}H$ were Golgi stained and analyzed for structural changes in hippocampal neurons. Advantages of the Golgi–Cox method for assessing dendritic spine dynamics are its resistance to fading or photobleaching over time. Often cited disadvantages of Golgi–Cox staining are the limited ability to determine the neurochemical phenotypes of impregnated neurons. However, the Golgi-Cox method has been described as a useful tool in a variety of human diseases and animal models, where data from gross inspection or histology was not consistent with the expected behavioral/neurologic alteration.(14, 15)

Immediately after sacrifice, brains (n = 6) were extracted and bilaterally cut along the mid-sagittal plane, then brains were treated with the Golgi-Cox method of staining. Right hemispheres were immersed for 2 weeks in an impregnation solution containing potassium dichromate and mercuric chloride. Samples were then immersed for at least 48 hours in a post-impregnation buffer. Each sample was sectioned at 200 μm in 1X PBS with a microtome. Samples were then transferred into wells and washed with 0.01 M PBS buffer (pH 7.4) with Triton X-100 (0.3%) (PBS-T). Immediately after washing, samples were stained with ammonium hydroxide and then immersed in a post-staining buffer (Bioenno Tech superGolgi kit). Sections were again washed in PBS-T, mounted on 1% gelatin-coated slides, and allowed to dry. Sections were finally dehydrated with ethanol solutions, followed by cleaning in xylene, and coverslipped with Permount™ (Fisher).

Dendritic Spine Density and Spine Morphology

Blinded to the experimental conditions, we analyzed dendritic spines that were conducted on coded Golgi impregnated brain sections that contained the dorsal hippocampus. Spines were examined on dendrites of dentate gyrus (DG) granule neurons as well as apical (stratum

radiatum) and basal (stratum oriens) dendrites of CA1 pyramidal neurons. The neurons that satisfied the following criteria were chosen for analysis in each of the experimental groups: presence of 1) non-truncated dendrites; 2) consistent and dark Golgi staining along the entire extent of the dendrites; and 3) relative isolation from neighboring neurons to avoid interference with analysis.(16) Five dendritic segments (each at least 20 nm in length(17)) per neuron were analyzed, and 6-7 neurons were analyzed per brain. Neurons that met staining criteria were traced using a 100 X oil objective, a computerized stage, and Neurolucida software (Ver. 11, Microbrightfield, Inc., Williston, VT).

Dendritic Morphology Quantification

The explored morphological characteristics included Sholl analysis, total dendritic length, number of branch points, and dendritic complexity index (DCI), and these were performed with the Neuroexplorer component of the Neurolucida program. First, we collected the Sholl analysis, which is used to assess the amount and distribution of the arbor at increasing radial distances from the cell body.(18) The distance between each radius was set to 10μ for our experiments. The length of each dendritic branch, within each progressively larger circle, is counted from the soma. This provides information about the amount and distribution of dendritic material. Next, we performed branch-point analyses. A branch point represents a bifurcation of the dendrite when a branch divides into two sub-branches. Branch-point analysis is based on the number of bifurcations and the order of the points.(19) Lower branch-point orders represent proximal regions of the tree, whereas larger branch-point orders characterize distal regions. The branch-point analysis was used to determine the complexity of the dendritic arborization. The complexity of the dendritic tree is an important phenotypic component of the branching analysis. DCI was determined by the following equation, DCI=∑ branch tip orders + # branch tips) x (total dendritic length/total number of primary dendrites). In the CA1 areas, apical and basal dendrites were analyzed separately.

Statistical Analysis

Data were expressed as a mean ± the standard error of the mean. The behavioral data were analyzed over the full 5-minute length of each test. A one-way ANOVA followed by a Bonferroni post-hoc test was used to evaluate statistical differences between sham and irradiated groups in the Y-maze. Unpaired two-tailed t-tests with Welch's correction were used to evaluate statistical differences between sham and irradiated groups. qRT-PCR was performed in triplicates and averaged prior to statistical analyses, such that the standard error of the mean applied only to the appropriate n, and not the triplicates. All statistical analyses were conducted with GraphPad Prism 6.0 software (La Jolla, CA), and $p < 0.5$ was considered significant. For measures of dendritic intersections, a mixed-factors ANOVA was used to test for the effects of irradiation (between subjects variable) and distance from the cell body (Sholl radius, repeated measures variable), and this was followed by a Fisher least significant difference post-hoc tests when appropriate.

RESULTS

Behavior

The Y-maze test is based on the instinctive curiosity of rodents to explore novel areas without negative or positive reinforcements to the animals.(20) In our study, sham irradiated mice exhibited a significant preference for the novel arm over the familiar and start arm, indicating normal spatial recognition ($F_{(2,27)} = 22.28$, $P < 0.0001$; Fig 1a). In contrast, the mice irradiated with $^{1}H + ^{16}O$ spent a significantly higher proportion of time exploring the familiar arm ($F_{(2.26)} = 6.15$, $P < 0.01$; Fig 1b), suggesting that they did not recognize the novel arm, which would indicate impaired spatial-recognition memory. Discrimination ratios can be interpreted as the animal 'forgetting' what arm was encountered during the familiarization phase, and a decrease in the discrimination ratio can occur either from increased exploration of the familiar arm or reduced exploration of the novel arm. (21) A group difference effect on recognition memory was expected and, indeed, the results showed a statistically significant treatment effect on the discrimination ratios ($t=3.83$, $P<0.01$). The $^{1}H + ^{16}O$-irradiated animals spent significantly more time exploring the familiar objects; hence, the discrimination ratio was negative (Fig. 1c) and the percentage of total entries to the novel arm was significantly lower ($t=4.95$, $p=.0001$; Fig 1d). No significant locomotor activity changes were observed due to irradiation. However, trends in significance towards increased locomotor activity due to treatment were found in measures of mean velocity ($t=2.04$, $p=.06$; Fig 2a), and total distance moved ($t=2.01$, $p=.07$; Fig 2b).

Modifications in NMDA and AMPA Receptor Expression

In this study, we examined the mRNA expression of N-methyl-D-aspartate (NMDA) subunits, Nr1, Nr2a, and Nr2b, in the hippocampus of sham and $^{1}H + ^{16}O$ irradiated mice. We found that the mRNA expression level in Nr1 did not significantly change due to treatment ($t=2.03$, $p=0.06$; Fig. 3a). However, we did find that irradiation significantly increased mRNA expression of subunit Nr2a ($t=2.31$; $p < 0.05$; Fig. 3b), but significantly decreased expression of subunit Nr2b ($t=5.13$, $p< 0.001$; Fig 3c).

We also evaluated the mRNA expression of a-amino-3-hydroxy-5-methyl-4-isoxazole propionic acid (AMPA) subunits, GluRl and GluR2. mRNA expression of GluRl significantly increased in irradiated animals ($t=2.80$, $p < 0.05$; Fig 4a), but mRNA expression of GluR2 showed no significant changes ($t=1.42$, $p=0.18$; Fig 4b).

Alterations in Presynaptic and Postsynaptic Expression

We analyzed the mRNA expression of presynaptic (synapsin-1 and synaptophysin) and postsynaptic markers (drebrin, synapse-associated protein 97, and PSD-95). $^{1}H + 160$ significantly increased mRNA expression in synapsin-1 ($t=4.95$, $p < 0.001$; Fig 5a) and synaptophysin ($t=2.38$, $p < 0.05$; Fig 5b). $^{1}H + ^{16}O$ also significantly increased drebrin ($t=4.06$, $p < 0.01$; Fig 5c) and synapse-associated protein 97 ($t=4.27$, $p < 0.01$; Fig 5d) mRNA expression, but PSD-95 ($t=0.15$, $p= 0.88$) was not affected.

Changes in Spine Density and Spine Morphology

Quantitative analysis showed that after $^{1}H + ^{16}O$ irradiation the overall spine density in the DG was not significantly changed ($t = 1.27$, $p = 0.23$; Table 1). Next, we analyzed the density of different types of dendritic spines, and we found that the density of thin spines was not significantly modulated ($t=0.09$, $p = 0.93$; Table 1). However, when we analyzed density by spine type, there was a significant increase in stubby spines ($t=2.91$, $p < 0.05$; Table 1), and a decrease in mushroom spines ($t=3.90$, $p < 0.01$, Table 1) after irradiation.

In contrast to what was observed in the DG spine analysis, irradiation significantly increased overall density in the CA1 apical spines ($t=3.82$, $p < 0.05$; Table 2a). In addition, when we analyzed the density by spine type, we did not find significant changes in thin ($t=0.28$, $p=0.79$ Table 2a) or stubby ($t= 1.17$, $p=0.30$ Table 2a) spine types. However, there was a significant decrease in the density of mushroom spines ($t=2.74$, $p < 0.05$; Table 2a). In the basal pyramidal dendrites of the CA1 region, overall spine density was unchanged after irradiation ($t=0.14$, $p=0.89$; Table 2b). There were also no significant changes in thin ($t=0.05$, $p=0.96$; Table 2b), stubby (t=l .48, $p=0.19$; Table 2b), or mushroom spines (t=l .76, $p= 0.15$; **see** table 2b).

Dendritic Morphology

Dentate Gyrus Granule Neurons.—To further investigate the effects of whole-body irradiation on neuronal morphology, we performed a segmental Sholl analysis to examine the changes in dendritic length as a function of radial distance from the cell soma. In the DG, there was a significant interaction between treatment and segmental dendritic length after irradiation ($F_{(25,78)} = 2.88$ $p<0.001$), indicating that the effect of irradiation is associated with a different distribution of dendritic branches over the entire tree. The ANOVA also detected a significant main effect of treatment ($F_{(1,78)} = 67.49$; $p <0.0001$) and distance ($F_{(25,78)} = 48.35$; $p <0.0001$). Post-hoc analysis revealed that irradiation increased dendritic arborization compared to the sham controls. This increase in arborization was particularly evident at 80μ, 160 – 180μ (Fisher's LSD, $p<0.05$) and at 100 – 150μ from the soma (Fisher's LSD, $p<0.001$; Fig 6a). In addition, we found differences in total dendritic length ($t=2.53$, $p < 0.05$ **see** Table 1) and a trend in the number of branch points ($t=2.34$ $p = 0.05$; **see** Table 1). In accordance, the DCI of the DG was significantly different between the groups ($t=3.30$, $p < 0.05$; Fig 6b).

CA1 Pyramidal Neurons.—We performed a similar analysis on the apical and basal region of the CA1 pyramidal neurons. There was a significant interaction between treatment and segmental dendritic length in the CA1 apical area ($F_{(24,104)} = 4.26$: $p<0.0001$). A two-way ANOVA also detected a significant main effect of treatment ($F_{(1,104)} = 160.8$; $p <0.0001$) and distance ($F_{(25,104)} = 43.20$; $p <0.0001$). Further analysis showed that radiation-induced alterations of apical dendrite morphology depended on radial distance from the soma. Sholl analysis of dendritic arborization revealed that irradiation significantly decreased intersections at 40–100 μm (Fisher's LSD, $p<0.0001$; Fig 7a) from the soma. In addition, arborization was significantly decreased in regions at 30 and 110–120 μm from the soma (Fisher's LSD, $p < 0.05$) in irradiated mice (Fig 7a).

In the basal dendrites of CA1 pyramidal cells, there was a significant interaction between treatment and sham segmental dendritic length ($F_{(25,104)} = 5.79$; $p < 0.0001$). An ANOVA also detected a main effect of treatment ($F_{(1,104)} = 50.92$; $p < 0.001$) and distance ($F_{(25,104)} = 180.30$; $p < 0.0001$). Post-hoc analysis revealed that irradiation decreased dendritic arborization at 30 - 40 μm and 100 μm from the soma (Fisher's LSD, $p<0.05$; Fig 7b) as well as at 50-90 μm (Fisher's LSD, $p<0.001$) compared to the sham controls (Fig 7b).

Similar to the observations in the DG, we found significant differences in the CA1 apical area and a trend towards significance in the basal area for total dendritic length (apical $t=5.23$, $p < 0.01$; basal $t=2.17$, $p=.06$), significant differences in the number of branch points (apical $t=3.18$, $p < 0.05$; basal $t=3.07$, $p < 0.05$ **see** table 2b), and the branch point complexity (apical $t=6.35$, $p < 0.001$, Fig 7c; basal $t=3.05$, $p < 0.05$, Fig 7d).

DISCUSSION

Exposure to $^{1}H + ^{16}O$ radiation induced numerous changes to the hippocampus of mice. Mice exposed to $^{1}H + ^{16}O$ radiation failed to significantly distinguish the novel arm from the familiar arm, showed a decreased arm discrimination ratio, spent less time exploring the novel object, and showed a reduced percentage of novel arm entries, relative to sham-irradiated mice in the Y-maze test (Fig 1). This indicates a deficit in short-term recall, a hippocampus-dependent process.(22) Expression of the NMDA receptor subunit, Nr2a, significantly increased, whereas Nr2b decreased. The expression of AMPA receptor subunit, GluR1, also significantly increased (Fig 4). Presynaptic density markers, synaptophysin and synapsin-1, underwent significant upregulation in irradiated mice, as did postsynaptic markers, drebrin-1 and synapse-associated protein 97 (Fig 5).

Irradiation also modulated hippocampal spine density by increasing the amount of stubby spines and decreasing the amount of mushroom spines in the DG. The apical CA1 region underwent a significant decrease in the density of mushroom spines as well as an overall increase in total spine density (**see** Table 2). Furthermore, the hippocampal dendritic arbor underwent remodeling. Dendritic length from the soma and DCI appear to have been altered, and a trend towards significance in bifurcations was observed in the DG granule neurons of treated animals. Similar changes were observed in the CA1, where basal dendrites underwent overall changes in complexity and bifurcations, and trended in total dendritic length. Apical CA1 dendrites decreased in overall length from the soma, complexity, and the number of branch points. (**see** Table 2)

Spatial learning and memory are considered hippocampus-dependent tasks.(23, 24) Previous studies examining the cognitive deficits from either ^{1}H or ^{16}O radiation exposure found that this exposure caused behavioral abnormalities.(5, 10, 11) Rats irradiated with .5 Gy of ^{16}O spent significantly less time exploring the novel object in the NOR paradigm.(10) Mice exposed to .3 Gy of ^{16}O showed a significant decrease in the discrimination index in the NOR test and in the object in place test.(5) Mice irradiated with .5 Gy of ^{1}H showed a significantly increased swim distance to the hidden platform during the spatial-2 reversal learning phase of the MWM test.(11) As previously stated, the only other study examining the effects of ^{1}H and HZE particles studied mice exposed to ^{1}H (.1Gy) and ^{56}Fe (.5Gy)

separated by 24 hours. The study found that mice were unable to distinguish between the novel and familiar objects in an NOR test 3 months postirradiation; however, the impairment was attributed to ^{1}H alone.(12) Therefore, it is thus possible that charged particle irradiation-induced deficits to hippocampal-dependent processes may depend on particle type, order of, dosage, and time between charged particle administration.

Hippocampal-dependent learning involves the tightly regulated synaptic interactions of presynaptic glutamatergic axons and postsynaptic dendritic spines. Dendrites are the branch-like extensions from neural cell bodies, which receive synaptic inputs, modulating action-potentials. Dendritic branches serve as computational units because of their ability to reach appropriate input targets, elicit action-potentials modulated by dendritic membrane potentials and to propagate action potentials to the soma.(25, 26) Each dendrite features a number of different spines that protrude from the dendritic shaft via actin scaffolding and serve to receive synaptic inputs.(27) The various types of dendritic spines are characteristic of the strength of the synapse. Mushroom and stubby spines, for example, are distinguished by their head surface area, which allows for more receptor anchoring. Because of their strong excitatory potential, mushroom and stubby spines are more stable and are able to last for longer periods of time, thus earning the role of memory spines. On the contrary, thin spines, which have a small bulbous head, are unstable but can be remodeled into stable spines. Because of this plasticity, thin spines are referred to as learning spines.(28) The decrease in DG and CA1 apical mushroom spines is consistent with the observed behavior of irradiated mice that showed diminished memory and recall during the Y-maze test. The increase in stubby spines observed in the DG could possibly be the result of localized changes in the GTPase activation pathway, which dictate the actin dynamic effectors responsible for the fine-tuning of spine neck morphology.(29) Accordingly, alterations to this pathway are observed in patients with various forms of mental retardation.(30, 31) However, this change was not observed in other hippocampal regions, and is a potential subject for future studies.

Dendritic spines are host to a number of ionotropic glutamate receptors. These include NMDA receptors coupled with AMPA receptors that, depending upon stimulation and postsynaptic density protein (PSD-95) presence, can dictate the spine morphology and induce long-term potentiation.(32–35) Also essential for synapse formation are presynaptic vesicle formation and clustering, which are regulated by synapsin-1.(36) Changes in dendritic spine and branching morphology disrupt neuronal circuits and are linked to many psychiatric disorders.(37–41) Acute stress and learning processes alike require reorganization of neural networks due to the tightly controlled nature of dendritic maintenance. (42)

HZE irradiation has been shown to modify dendritic morphology within the prefrontal cortex and hippocampus. HZE particles appear to modulate spine density, dendritic length, and bifurcations. Dendritic spines also appear to undergo changes in proportions of subtypes.(8, 43) A decrease in dendritic length, branch point, and spine density are apparent in the DG of ^{1}H-irradiated mice receiving doses of .1 and 1 Gy one month post-exposure. (44) We observed the opposite effect in the DG, where irradiation caused an increase in dendritic length, a trend towards increase in total branch points, and cranial gamma-

irradiation has been previously shown to increase NMDA receptor subunits NR1 and NR2A in the CA1 of rats. (45) We observed a trend towards fold increase in NR1 expression in the hippocampus, which is consistent with these findings; however, the decrease of NR2A expression is not. Interestingly, an increase in PSD-95 expression has been previously observed as a result of ^{16}O irradiation (.05 and .3 Gy, 6-weeks postexposure) in the medial prefrontal cortex.(5) An increase in PSD-95 expression was also observed after ^{1}H irradiation (.1 and 1 Gy, 30 days postexposure) in the DG, though we did not observe a change in PSD-95 mRNA expression in the whole hippocampus.(44) It is unclear whether the effects of charged-particle irradiation on PSD-95 expression are due to transcription, radiation dosage, age of exposure, or length of time postexposure. However, treated animals saw a significant increase in expression of two other post-synaptic markers, synapse-associated protein-97 and drebrin-1.

It has been previously reported that ^{56}Fe irradiation (.5 Gy) caused a decrease in dendritic length at approximately 90-140 μm from the soma, and that (.1 and lGy) resulted in an overall decrease in dendritic length in the DG.(43) However, our Sholl analyses showed that a significant increase in dendritic length at 90-180μ from the soma in the DG, and an increase in complexity, yet the proportion of mushroom spines decreased, and stubby spines increased. We found an irradiation-induced decrease in dendritic length in the basal and apical CA1 areas at approximately 30-100 and 30-110 μm from the soma, respectively. In addition, we observed severely reduced dendritic complexity in the basal and apical CA1, a decrease in apical mushroom spine density, an increase in overall spine density suggesting a shift toward long-term depression, which likely resulted in modulation of the hippocampal circuit output. Other studies have recently found that mice 3-months postexposure to ^{28}Si ion radiation (1 Gy), and ^{1}H radiation (.5 Gy, 1 Gy) suffered impairments to CA1-region neuronal outputs.(46, 47) ^{1}H-irradiated (1Gy) mice exhibited hyperpolarization of the resting membrane potential, a decrease in input resistance, an increase in persistent Na+ current and increased rate of miniature excitatory postsynaptic currents in CA1 neurons.(4d) A lower dose of ^{1}H (.5 Gy) evoked increased field excitatory post-synaptic potentials and reduced spontaneous oscillation frequency in the CA1 9 months postirradiation.(11) Exposure to ^{28}Si resulted in decreased population spike amplitudes and reduced maximal neuronal output.(47) The DG is considered the input region of the tri-synaptic hippocampal circuit, where information flows from the DG to CA3, and ultimately to the CA1, which serves as the main output.(48, 49) Complex morphological changes associated with different subregions may ultimately compromise the output of hippocampal-dependent processes, potentially manifesting in cognitive-behavioral deficits. The CA1 region of the hippocampus has been implicated in signaling environmental novelty, and thus, the observed morphological changes to the dendritic arbor along with the changes in spine densities and subtypes within the DG and CA1 may have significantly compromised this ability in irradiated mice.(50)

Accumulating evidence suggests deep-space radiation-induced cognitive hazards associated with dendritic remodeling and synapse-related protein expression in cognitive structures within the brain. Dendrites serve as key computational units necessary for processing targeted inputs and relaying signals to the soma.(25) In this study, one of the first to investigate the biological effects of exposure to two charged particles within a day, $^{1}H + ^{16}O$

irradiation resulted in short-term memory deficits, dendritic remodeling within the DG and CA1 of the hippocampus, and changes in gene expression of synaptic markers. Due to reported differences in behavior as a result of exposure to different particles and energies, further research with true and more complex mixed fields is required. Although there is a growing understanding of the effects of charged particle irradiation on the CNS, the body of literature pertains almost exclusively to studies done with male rodents. Due to inherent differences in sex-dependent radiosensitivity, future studies should address comparisons between males and females. Finally, glial cells play an important role in the maintenance of neurons. There are currently no publications examining changes in oligodendrocytes or astrocytes due to whole-body exposure to ^{1}H and other HZE particles in animal models.

ACKNOWLEDGEMENTS

This work was supported by NSBRI Grant RE03701 thru NCC 9-58. The funders had no role in study design, data collection and analysis, decision to publish, or preparation of the manuscript. This work was also supported by Core Facilities of the Center for Translational Neuroscience IDeA program award P30 GM110702.

Funding: This work was supported by NSBRI Grant RE03701 thru NCC 9-58. The funders had no role in study design, data collection and analysis, decision to publish, or preparation of the manuscript.

References

1. Badhwar GD, O'Neill PM. Long-term modulation of Galactic Cosmic Radiation and its model for space exploration. Advances in space research : the official journal of the Committee on Space Research. 1994;14(10):749–57. Epub 1994/10/01.
2. Townsend Laurence W., B GD, Blakely Eleanor A., Braby Leslie A., Cucinotta Francis A.,Curtis Stanley B., Michael Fry RJ, Land Charles E., Smart Don F.. NCRP Report No. 153 Information. U.S. Library of Congress: National Council on Radiation Protection and Measurements, 2006 153.
3. Kokhan VS, Matveeva MI, Mukhametov A, Shtemberg AS. Risk of defeats in the central nervous system during deep space missions. Neuroscience and biobehavioral reviews. 2016;71:621–32. Epub 2016/10/30. [PubMed: 27756690]
4. Hassler DM, Zeitlin C, Wimmer-Schweingruber RF, Ehresmann B, Rafkin S, Eigenbrode JL, et al. Mars' surface radiation environment measured with the Mars Science Laboratory's Curiosity rover. Science. 2014;343(6169):1244797 Epub 2013/12/11. [PubMed: 24324275]
5. Zeitlin C, Hassler DM, Cucinotta FA, Ehresmann B, Wimmer-Schweingruber RF, Brinza DE, et al. Measurements of energetic particle radiation in transit to Mars on the Mars Science Laboratory. Science. 2013;340(6136):1080–4. Epub 2013/06/01. [PubMed: 23723233]
6. Gregory Nelson LS, Janice Huff. Evidence Report: Risk of Acute and Late Central NervousSystem Effects from Radiation Exposure. [NASA Evidence Report] 2016 [updated 4/16/2016]; Available from: https://humanresearchroadmap.nasa.gov/Evidence/reports/CNS.pdf.
7. Nelson GA. Space Radiation and Human Exposures, A Primer. Radiation research.2016;185(4):349–58. [PubMed: 27018778]
8. Parihar VK, Allen B, Tran KK, Macaraeg TG, Chu EM, Kwok SF, et al. What happens toyour brain on the way to Mars. Sci Adv. 2015;1(4). Epub 2015/07/17.
9. Shukitt-Hale B, Casadesus G, McEwen JJ, Rabin BM, Joseph JA. Spatial learning andmemory deficits induced by exposure to iron-56-particle radiation. Radiation research. 2000;154(1):28–33. Epub 2000/06/17. [PubMed: 10856962]
10. Rabin BM, Poulose SM, Carrihill-Knoll KL, Ramirez F, Bielinski DF, Heroux N, et al.Acute Effects of Exposure to (56)Fe and (16)O Particles on Learning and Memory. Radiation research. 2015;184(2):143–50. Epub 2015/07/25. [PubMed: 26207687]
11. Bellone JA, Rudobeck E, Hartman RE, Szucs A, Vlkolinsky R. A Single Low Dose of Proton Radiation Induces Long-Term Behavioral and Electrophysiological Changes in Mice. Radiation research. 2015;184(2):193–202. Epub 2015/07/25. [PubMed: 26207690]

12. Raber J, Allen AR, Sharma S, Allen B, Rosi S, Olsen RH, et al. Effects of Proton and Combined Proton and (56)Fe Radiation on the Hippocampus. Radiation research. 2016;185(1):20–30. Epub 2016/01/01. [PubMed: 26720797]
13. Soares E, Prediger RD, Nunes S, Castro AA, Viana SD, Lemos C, et al. Spatial memory impairments in a prediabetic rat model. Neuroscience. 2013;250:565–77. Epub 2013/08/06. [PubMed: 23912035]
14. Mikolaenko I, Rao LM, Roberts RC, Kolb B, Jinnah HA. A Golgi study of neuronal architecture in a genetic mouse model for Lesch-Nyhan disease. Neurobiology of disease. 2005;20(2):479–90. Epub 2005/05/24. [PubMed: 15908225]
15. Ramakers GJ, Wolfer D, Rosenberger G, Kuchenbecker K, Kreienkamp HJ, Prange-Kiel J, et al. Dysregulation of Rho GTPases in the alphaPix/Arhgef6 mouse model of X-linked intellectual disability is paralleled by impaired structural and synaptic plasticity and cognitive deficits. Human molecular genetics. 2012;21(2):268–86. Epub 2011/10/13. [PubMed: 21989057]
16. Titus AD, Shankaranarayana Rao BS, Harsha HN, Ramkumar K, Srikumar BN, Singh SB, et al. Hypobaric hypoxia-induced dendritic atrophy of hippocampal neurons is associated with cognitive impairment in adult rats. Neuroscience. 2007;145(1):265–78. Epub 2007/01/16. [PubMed: 17222983]
17. Magarinos AM, Li CJ, Gal Toth J, Bath KG, Jing D, Lee FS, et al. Effect of brain-derived neurotrophic factor haploinsufficiency on stress-induced remodeling of hippocampal neurons. Hippocampus 2011;21(3):253–64. Epub 2010/01/23. [PubMed: 20095008]
18. Sholl DA. Dendritic organization in the neurons of the visual and motor cortices of the cat. J Anat. 1953;87(4):387–406. Epub 1953/10/01. [PubMed: 13117757]
19. Morley BJ, Mervis RF. Dendritic spine alterations in the hippocampus and parietal cortex ofalpha7 nicotinic acetylcholine receptor knockout mice. Neuroscience. 2013;233:54–63. Epub 2012/12/29. [PubMed: 23270857]
20. Sarnyai Z, Sibille EL, Pavlides C, Fenster RJ, McEwen BS, Toth M. Impaired hippocampal-dependent learning and functional abnormalities in the hippocampus in mice lacking serotonin(1A) receptors. Proceedings of the National Academy of Sciences of the United States of America. 2000;97(26):14731–6. Epub 2000/12/20. [PubMed: 11121072]
21. Burke SN, Wallace JL, Nematollahi S, Uprety AR, Barnes CA. Pattern separation deficitsmay contribute to age-associated recognition impairments. Behavioral neuroscience. 2010;124(5):559–73. Epub 2010/10/14. [PubMed: 20939657]
22. Shu SY, Jiang G, Zeng QY, Wang B, Li H, Ma L, et al. The marginal division of the striatum and hippocampus has different role and mechanism in learning and memory. Molecular neurobiology. 2015;51(2):827–39. Epub 2014/10/03. [PubMed: 25274077]
23. Moser E, Moser MB, Andersen P. Spatial learning impairment parallels the magnitude of dorsal hippocampal lesions, but is hardly present following ventral lesions. The Journal of neuroscience : the official journal of the Society for Neuroscience. 1993;13(9):3916–25. Epub 1993/09/01. [PubMed: 8366351]
24. Morris RG, Schenk F, Tweedie F, Jarrard LE. Ibotenate Lesions of Hippocampus and/or Subiculum: Dissociating Components of Allocentric Spatial Learning. The European journal of neuroscience. 1990;2(12):1016–28. Epub 1990/01/01. [PubMed: 12106063]
25. Tavosanis G Dendritic structural plasticity. Developmental neurobiology. 2012;72(1):73–86. Epub 2011/07/16. [PubMed: 21761575]
26. Moore JJ, Ravassard PM, Ho D, Acharya L, Kees AL, Vuong C, et al. Dynamics of corticaldendritic membrane potential and spikes in freely behaving rats. Science. 2017;355(6331). Epub 2017/03/11.
27. Koleske AJ. Molecular mechanisms of dendrite stability. Nature reviews Neuroscience. 2013;14(8):536–50. Epub 2013/07/11. [PubMed: 23839597]
28. Xu X, Miller EC, Pozzo-Miller L. Dendritic spine dysgenesis in Rett syndrome. Frontiers in neuroanatomy. 2014;8:97 Epub 2014/10/14. [PubMed: 25309341]
29. Govek EE, Newey SE, Van Aelst L. The role of the Rho GTPases in neuronal development. Genes & development. 2005;19(1):1–49. Epub 2005/01/05. [PubMed: 15630019]

30. Ebrahimi S, Okabe S. Structural dynamics of dendritic spines: molecular composition,geometry and functional regulation. Biochimica et biophysica acta. 2014;1838(10):2391–8. Epub 2014/06/11. [PubMed: 24915021]
31. Newey SE, Velamoor V, Govek EE, Van Aelst L. Rho GTPases, dendritic structure, and mental retardation. Journal of neurobiology. 2005;64(1):58–74. Epub 2005/05/11. [PubMed: 15884002]
32. Yudowski GA, Olsen O, Adesnik H, Marek KW, Bredt DS. Acute inactivation of PSD-95 destabilizes AMPA receptors at hippocampal synapses. PloS one. 2013;8(1):e53965 Epub 2013/01/24. [PubMed: 23342049]
33. Gonda X Basic pharmacology of NMDA receptors. Current pharmaceutical design. 2012;18(12):1558–67. Epub 2012/01/28. [PubMed: 22280436]
34. Opazo P, Sainlos M, Choquet D. Regulation of AMPA receptor surface diffusion by PSD-95 slots. Current opinion in neurobiology. 2012;22(3):453–60. Epub 2011/11/05. [PubMed: 22051694]
35. Ehrlich I, Malinow R. Postsynaptic density 95 controls AMPA receptor incorporation during long-term potentiation and experience-driven synaptic plasticity. The Journal of neuroscience : the official journal of the Society for Neuroscience. 2004;24(4):916–27. Epub 2004/01/30. [PubMed: 14749436]
36. Bykhovskaia M Synapsin regulation of vesicle organization and functional pools. Seminarsin cell & developmental biology. 2011;22(4):387–92. Epub 2011/08/11.
37. Flores G, Morales-Medina JC, Diaz A. Neuronal and brain morphological changes in animal models of schizophrenia. Behavioural brain research. 2016;301:190–203. Epub 2016/01/08. [PubMed: 26738967]
38. Frankfurt M, Luine V. The evolving role of dendritic spines and memory: Interaction(s) with estradiol. Hormones and behavior. 2015;74:28–36. Epub 2015/05/21. [PubMed: 25993604]
39. Emoto K Dendrite remodeling in development and disease. Development, growth &differentiation. 2011;53(3):277–86. Epub 2011/04/16.
40. Mancuso JJ, Chen Y, Li X, Xue Z, Wong ST. Methods of dendritic spine detection: from Golgi to high-resolution optical imaging. Neuroscience. 2013;251:129–40. Epub 2012/04/24. [PubMed: 22522468]
41. Kulkarni VA, Firestein BL. The dendritic tree and brain disorders. Molecular and cellular neurosciences. 2012;50(1):10–20. Epub 2012/04/03. [PubMed: 22465229]
42. Qiao H, An SC, Ren W, Ma XM. Progressive alterations of hippocampal CA3-CA1 synapsesin an animal model of depression. Behavioural brain research. 2014;275:191–200. Epub 2014/09/07. [PubMed: 25192638]
43. Allen AR, Raber J, Chakraborti A, Sharma S, Fike JR. (56)Fe Irradiation Alters Spine Density and Dendritic Complexity in the Mouse Hippocampus. Radiation research. 2015;184(6):586–94. Epub 2015/11/19. [PubMed: 26579941]
44. Parihar VK, Pasha J, Tran KK, Craver BM, Acharya MM, Limoli CL. Persistent changes inneuronal structure and synaptic plasticity caused by proton irradiation. Brain structure & function. 2015;220(2):1161–71. Epub 2014/01/22. [PubMed: 24446074]
45. Shi L, Adams MM, Long A, Carter CC, Bennett C, Sonntag WE, et al. Spatial learning andmemory deficits after whole-brain irradiation are associated with changes in NMDA receptor subunits in the hippocampus. Radiation research. 2006;166(6):892–9. Epub 2006/12/08. [PubMed: 17149974]
46. Sokolova IV, Schneider CJ, Bezaire M, Soltesz I, Vlkolinsky R, Nelson GA. Proton radiation alters intrinsic and synaptic properties of CA1 pyramidal neurons of the mouse hippocampus. Radiation research. 2015;183(2):208–18. Epub 2015/01/27. [PubMed: 25621896]
47. Rudobeck E, Nelson GA, Sokolova IV, Vlkolinsky R. (28)silicon radiation impairs neuronal output in CA1 neurons of mouse ventral hippocampus without altering dendritic excitability. Radiat Res. 2014;181(4):407–15. Epub 2014/03/15. [PubMed: 24625098]
48. Amaral DG, Witter MP. The three-dimensional organization of the hippocampal formation: are view of anatomical data. Neuroscience. 1989;31(3):571–91. Epub 1989/01/01. [PubMed: 2687721]
49. Witter MP. The perforant path: projections from the entorhinal cortex to the dentate gyrus. Progress in brain research. 2007;163:43–61. Epub 2007/09/04. [PubMed: 17765711]

50. Larkin MC, Lykken C, Tye LD, Wickelgren JG, Frank LM. Hippocampal output area CA1broadcasts a generalized novelty signal during an object-place recognition task. Hippocampus. 2014;24(7):773–83. Epub 2014/03/07. [PubMed: 24596296]

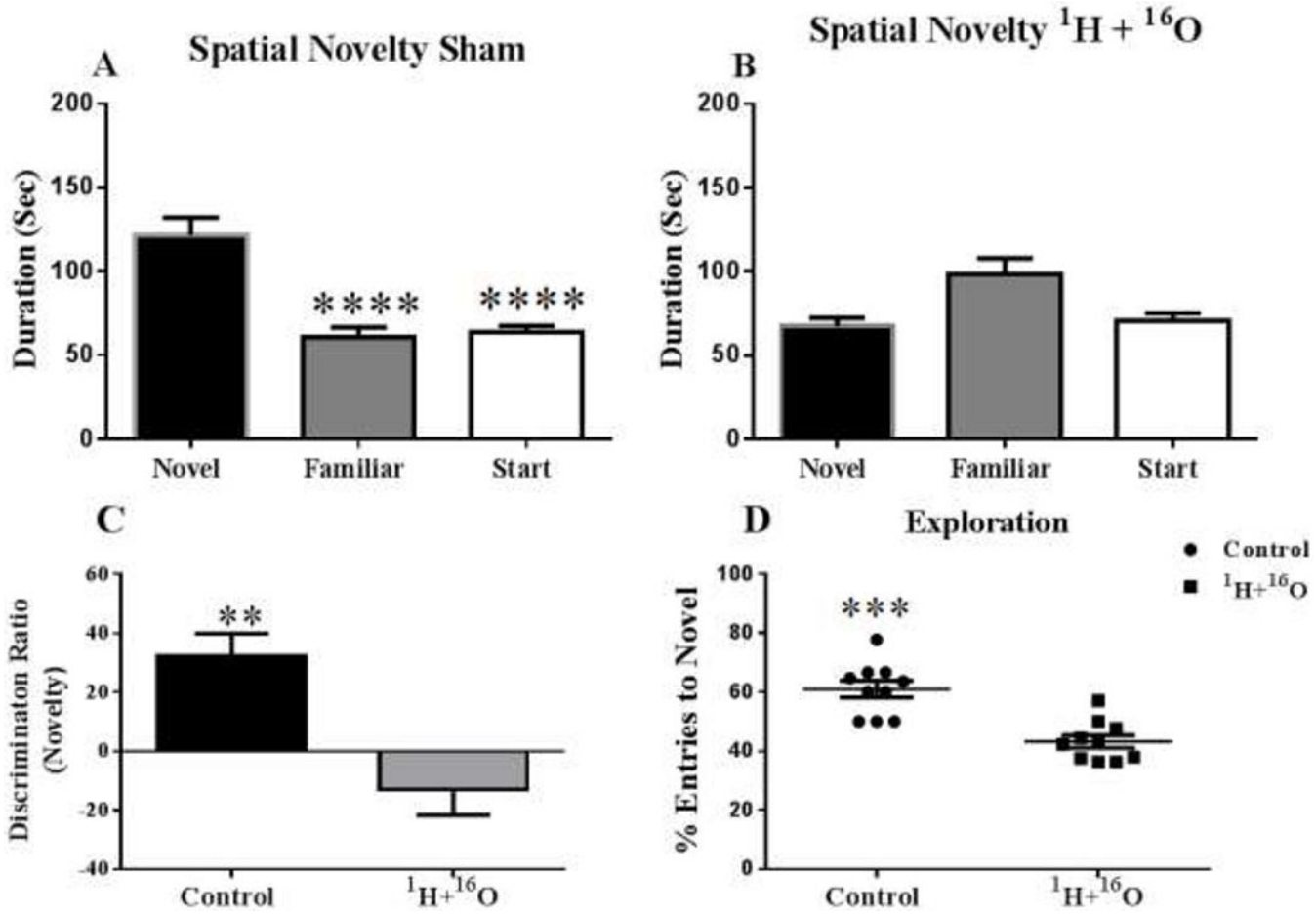

Figure 1: $^{1}H + ^{16}O$ irradiation impairs short-term memory during Y-maze test.

Mice exposed to radiation showed impaired memory during Y-maze testing, as compared to nonirradiated mice, by failing to recognize the novel environment when exposed to it 4 hours later (**A**, **B**). (**A**) Sham-irradiated mice were able to successfully distinguish the novel arm, by spending significantly more time exploring it. (**B**) Irradiated mice were not able to distinguish between the three Y-maze arms, and spent an approximately equal time exploring all arms during the retention trial. **(C)** $^{1}H + ^{16}O$ irradiated animals spent significantly more time exploring the familiar object than the novel object; thus, the discrimination ratio of the irradiated animals was below the zero axis. **(D)** Radiation also significantly decreased the total number of entries into the novel arm. Average ± SEM (n=10); *p<.05; **p<.01; ***p<001; ****p<.0001

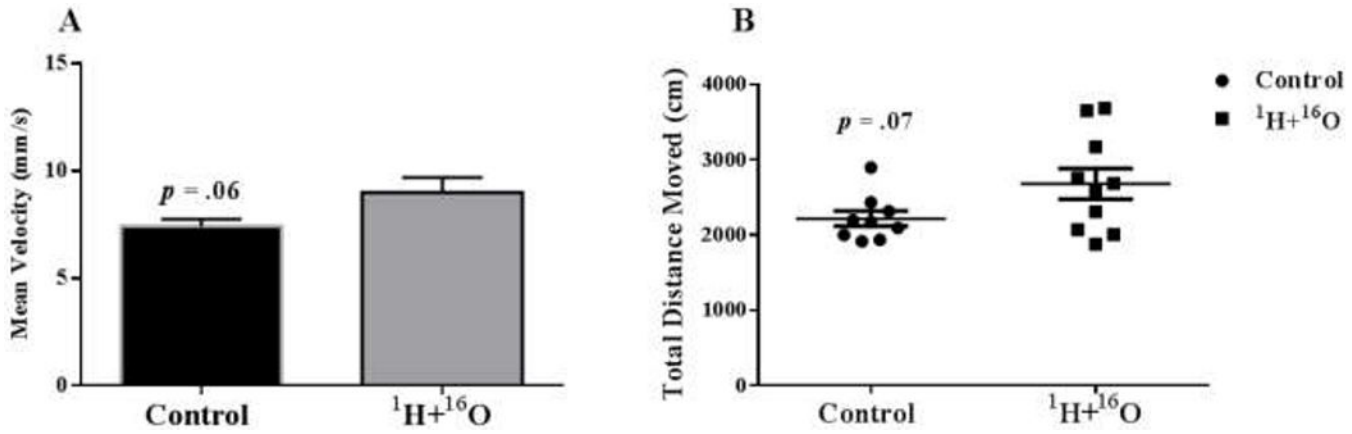

Figure 2: $^{1}H + ^{16}O$ irradiation causes trends toward significance in locomotor activity in the Y-maze test.

(A) $^{1}H + ^{16}O$ irradiated animals displayed a trend towards increased mean velocity. **(B)** Radiation also displayed a trend towards increased total distance moved. Average ± SEM (n=10)

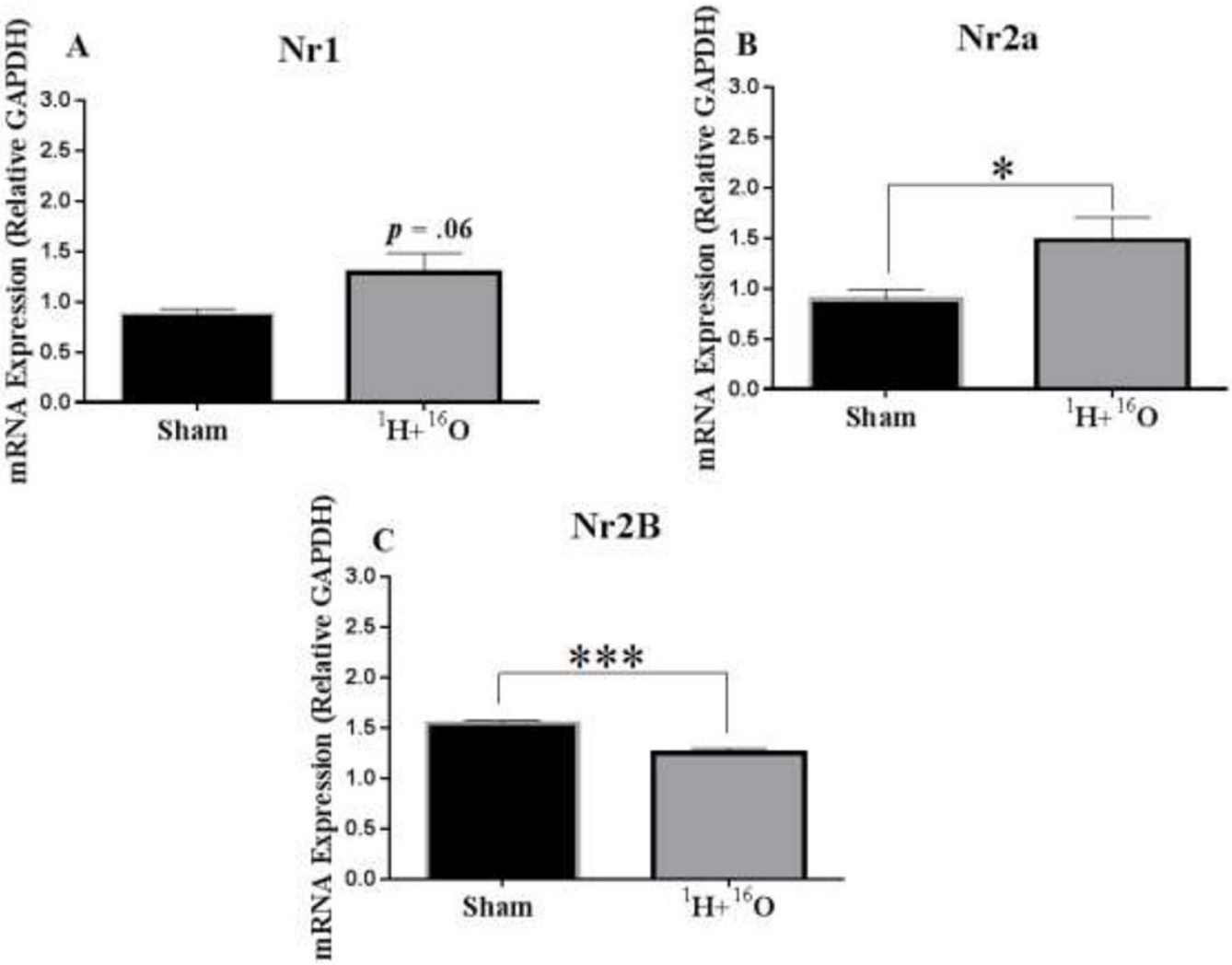

Figure 3: $^{1}H + ^{16}O$ radiation induces alterations in NMDA receptor gene expression.

(A) The mRNA levels of the NMDA subunit, Nr1, were not significantly changed in irradiated mice compared to sham mice. **(B)** However, the mRNA levels in the NMDA subunit, Nr2A, were significantly upregulated, **(C)** and the mRNA levels in NMDA subunit, Nr2B, were significantly decreased in irradiated mice compared to sham. Data are presented as fold change in gene expression relative to 0 Gy controls. Average ± SEM (n=10); *p < 0.05; ***p < 0.001

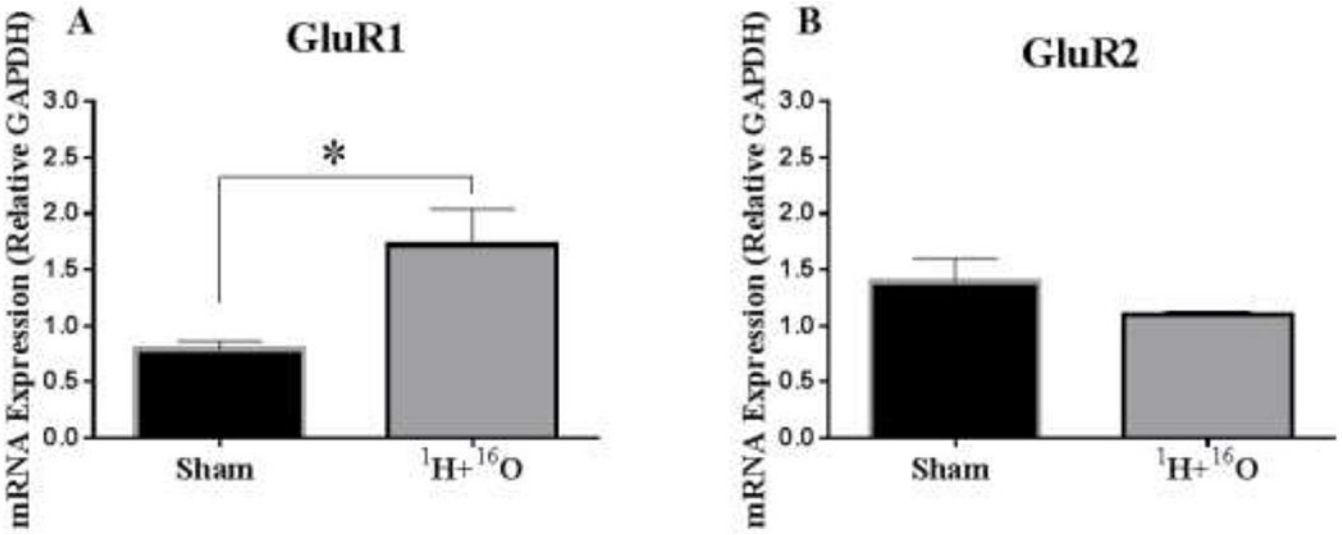

Figure 4: Effects of $^{1}H + ^{16}O$ exposure on gene expression of AMPA receptors.

(A) In irradiated mice, the mRNA expression level of AMPA subunit, GluR1, significantly increased compared to sham exposed mice; **(B)** however, the mRNA expression level in AMPA subunit, GluR2, decreased, but not significantly. Average ± SEM (n = 10); *p < 0.05.

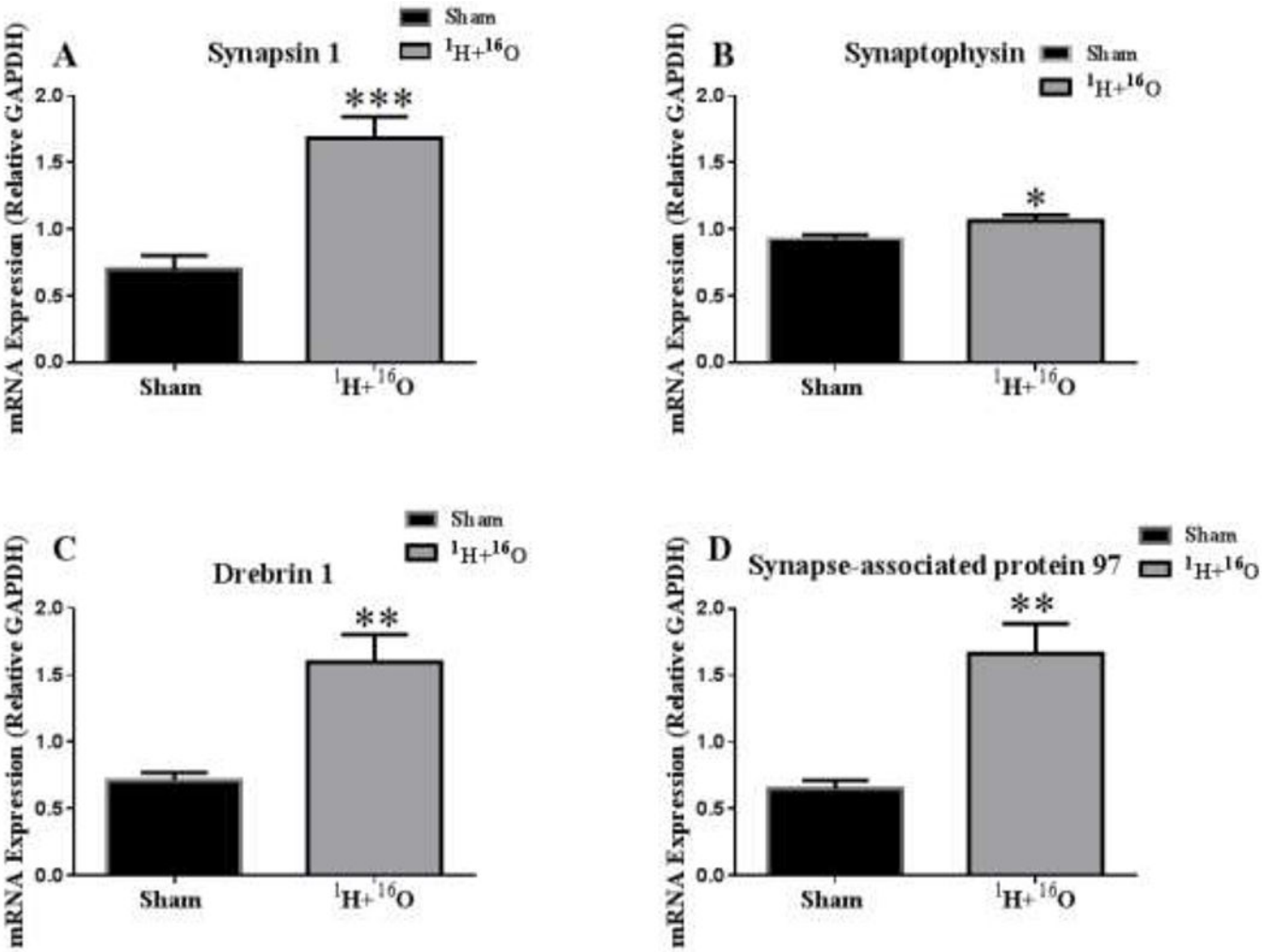

Figure 5: Alterations in presynaptic and postsynaptic gene expression.

(A) Synapsin 1 and (**B)** synaptophysin mRNA expression significantly increased in irradiated mice compared to sham irradiated mice. Postsynaptic markers **(C)** drebrin and **(D)** synapse-associated protein 97 also experienced significant increases after $^{1}H + ^{16}O$ exposure compared to sham irradiated mice. Average ± SEM (n = 10); *p < 0.05; **p < 0.01; ***p<.001

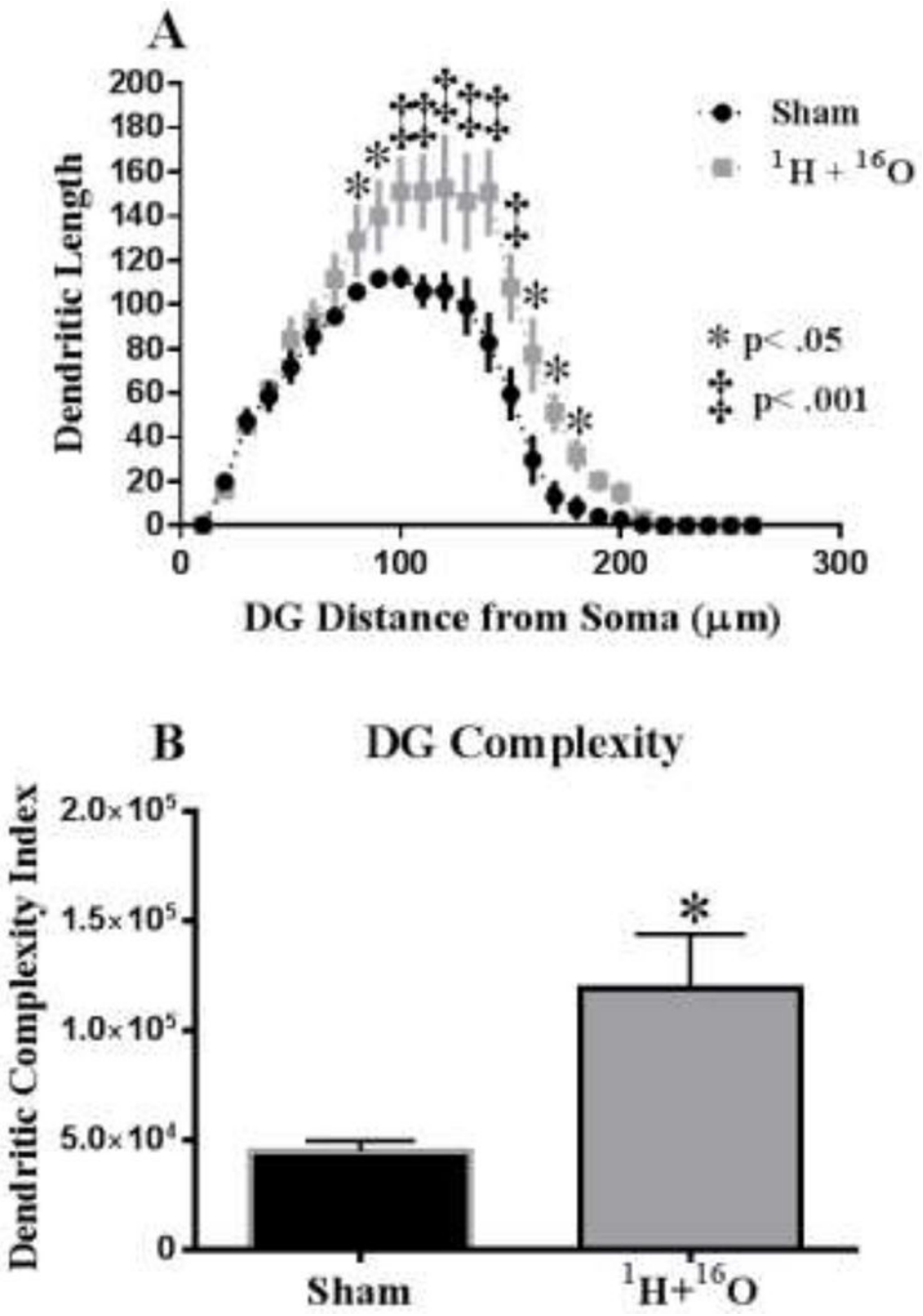

Figure 6: Sholl analyses and Dendrite Complexity of neurons in the dentate gyrus.

(A) Dendritic length, measured by Sholl analysis, increased in arborization, particularly evident at 80-180 μm from the soma. **(B)** $^{1}H + ^{16}O$ exposure greatly increased the overall dendrite complexity in the dentate gyrus. Average ± SEM (n = 5); *p < 0.05, ‡p < 0.001.

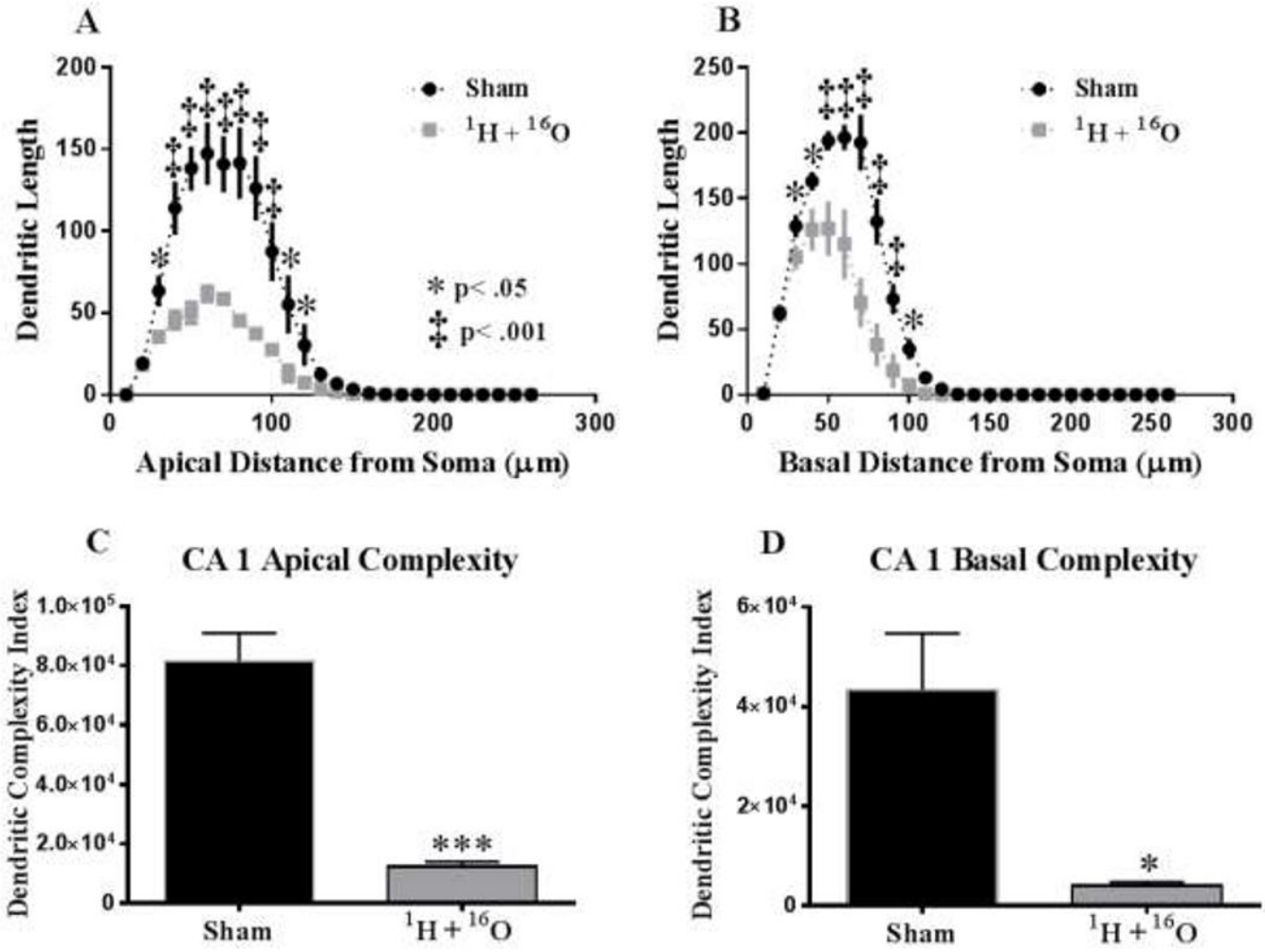

Figure 7: Sholl analyses and Dendrite complexity of CA1 pyramidal neurons.

(A) Sholl analysis revealed that irradiation significantly decreased dendritic length from the soma at 30-120 μm in the apical CA1. **(B)** Basal CA1 dendrites underwent a decrease in arborization at 30-100 μm from the soma in irradiated animals. **(C)** In the CA1 apical pyramidal dendrites, there was a significant decrease in the overall complexity. **(D)** $^{1}H + ^{16}O$ irradiation significantly decreased basal dendrite complexity. Average ± SEM (n = 5); *p < 0.5, **p < 0.01, ***p<0.001, ‡p < 0.001.

Table 1:

Effects of $^{1}H + ^{16}O$ on spine morphology in hippocampal DG

Cell Type and Measurement	Sham (mean ± SEM)	$^{1}H + ^{16}O$ (mean ± SEM)	*p*-value
DG			
Thin Spines	60.08 ± 2.24	59.85 ± 1.45	$p = 0.93$
Stubby Spines	**29.04 ± 0.82**	**33.64 ± 1.35**	***p < 0.05***
Mushroom Spines	**9.70 ± 0.80**	**6.51 ± 0.16**	***p < 0.01***
Overall Density	19.40 ± 0.46	20.23 ± 0.47	$p = 0.23$
Total Dendritic Length (μm)	1,269 ± 75.97	1,747 ± 191.3	***p < 0.05***
Total # Branch Points	10.92 ± 0.77	16.35 ± 2.45	*p = 0.05*
Dendritic Complexity	**44,955 ± 4592**	**119,171 ± 24,941**	***p < 0.05***

*Bold figures represent significant values

Table 2:

Morphological analysis of apical and basal dendrites in CA1

A			
Cell Type and Measurement	**Sham (mean ± SEM)**	**$^{1}H + ^{16}O$ (mean ± SEM)**	***p*-value**
CA1 Apical			
Thin Spines	57.09 ± 3.89	58.19 ± 0.76	$p = 0.79$
Stubby Spines	32.88 ± 2.51	35.93 ± 0.71	$p = 0.30$
Mushroom Spines	**10.03 ± 1.47**	**5.88 ± 0.36**	***p < 0.05***
Overall Density	**19.06 ± 0.47**	**21.52 ± 0.54**	***p < 005***
Total Dendritic Length (μm)	**860.0 ± 75.80**	**404.9 ± 15.55**	***p < 001***
Total # Branch Points	**13.80 ± 1.37**	**7.01 ɑ 1.63**	***p < 0.05***
Dendritic Complexity	**81,463 ± 9,499**	**12,348 ɑ 1,730**	***p < 0.001***
B			
Cell Type and Measurement	**Sham (mean ± SEM)**	**$^{1}H + ^{16}O$ (mean ± SEM)**	***p*-value**
CA1 Basal			
Thin Spines	55.44 ± 2.47	55.60 ± 1.82	$p = 0.96$
Stubby Spines	34.41 ± 0.98	37.65 – 1.96	$p = 0.19$
Mushroom Spines	10.15 ± 1.90	6.76 ± 0.34	*p = 0.15*
Overall Density	18.47 ± 0.64	18.63 ± 0.52	$p = 0.89$
Total Dendritic Length (μm)	1,326 ± 160.9	750.5 ± 209.9	*p = 0.06*
Total # Branch Points	**16.56 ± 1.72**	**7.87 ± 2.24**	***p < 0.05***
Dendritic Complexity	**43,333 ± 11,350**	**4.098 ± 694.2**	***p < 0.05***